Determination of alternative forest road routes using produced landslide susceptibility maps: A case study of Tonya (Trabzon), Türkiye

Fatih Kadı *1 [iD], **Osman Salih Yılmaz** 2 [iD]

1 Karadeniz Technical University, Department of Geomatics Engineering, Türkiye, fatihkadi@ktu.edu.tr
2 Manisa Celal Bayar University, Demirci Vocational School, Türkiye, osmansalih.yilmaz@cbu.edu.tr

Abstract

Firstly, Landslide Susceptibility Maps of the study area were produced using Frequency Ratio and Modified Information Value models. Nine factors were defined and the Landslide Inventory Map was used to produce these maps. In the Landslide Susceptibility Maps obtained from the Frequency Ratio and Modified Information Value models, the total percentages of high and very high-risk areas were calculated as 10% and 15%, respectively. To determine the accuracy of the produced Landslide Susceptibility Maps, the success and the prediction rates were calculated using the receiver operating curve. The success rates of the Frequency Ratio and Modified Information Value models were 82.1% and 83.4%, respectively, and the prediction rates were 79.7% and 80.9%. In the second part of the study, the risk situations of 125 km of forest roads were examined on the map obtained by combining the Landslide Susceptibility Maps. As a result of these investigations, it was found that 4.28% (5.4 km) of the forest roads are in very high areas and 4.27% (5.3 km) in areas with high landslide risk areas. In the last part of the study, as an alternative to forest roads with high and very high landslide risk, 9 new forest road routes with a total length of 5.77 km were produced by performing costpath analysis in with geographic information systems.

1. Introduction

Disasters are essentially different types of events, whether natural, technological, or human-induced, that have adverse consequences in terms of physical, economic, and social losses. These events have a significant impact on societies by disrupting normal life and are beyond the capability of local interventions to prevent [1]. There are many disasters that affect life in the world, and landslides are one of these types of disaster. Landslide: commonly defined as the movement or sliding of material, typically consisting of soil, rock, or their mixture, on the surface, often leading to human casualties and property loss, is a prevalent type of natural disaster [2, 3].

According to data from the Emergency Events Database (EM-DAT), it was reported that 765 individuals lost their lives due to landslides in Türkiye from 1923 to 2023, with a total of 14,740 people being affected by this calamity. Furthermore, an observation indicates that over half of the natural disasters occurring in Türkiye during the same period were geophysical in nature,

incorporating landslides [4]. In addition, it was also found that Trabzon province, which includes the study area, was the first province in Türkiye in terms of the number of landslides with 38 fatalities and 336 fatalities in terms of the number of incidents and fatalities [5]. To reduce the devastation caused by landslides, it is crucial to identify the areas at risk of potential landslides [6, 7].

One of the map types commonly used to identify potential landslide areas is the landslide susceptibility map (LSM) [8-22]. A LSM is a type of map that generally defines the relative susceptibility of areas within a region to landslide hazards [23-26]. The use of this type of map by local governments and practitioners in activities for various purposes (route and appropriate site selection, etc.) will make it possible to reduce the destructive power of landslide disasters.

Numerous scientific studies have investigated different methods for generation of LSMs. In [27] the models used to generate LSM were categorized into three different classes: based on physical, heuristics, and statistics. Physically depended on models employ mechanical rules to control slope stability. The most

important advantage of this model is that it can be used more efficiently than other models in cases where the data used to generate the LSM are missing or insufficient [27, 28]. In heuristic-based models, the factors used to produce the LSM are first identified. Each factor is then scored by experts by comparing it with other factors [28]. There are heuristic-based models such as the fuzzy logic approach [29-33] and the analytical hierarchy process [16, 30, 34-37]. Conversely, statistical models, intend to predict future landslide disasters by correlating previous landslides and the factors that triggered them. Logistic regression [38-44] frequency ratio (FR) method [16, 45-49], information value (IV) model [7, 26, 36, 50, 51] and the modified information value (MIV) [32, 52] are among the statistical models employed during the generation of LSM. FR and MIV models, which are statistical-based methods, ensure that the accuracy of the produced map is more reliable and understandable compared to other methods [53]. Therefore, FR and MIV methods have been used in many studies [54-59,52,60].

In forested areas affected by landslides, another at-risk element is forest roads [61-64]. Forest roads, which are the subject of the aim of the research, are the roads located in the forest area and allow the forests to be put into operation in a rational way by systematically penetrating every part of the forest. Forest roads are an important physical element for the implementation of forestry policies. In addition, these roads should be constructed in such a way as to cause the least damage to the stand, land and natural nature, and the maintenance, construction and transportation works of the roads should be investigated in a sensitive and detailed way to carry out the works at minimum cost [65]. The destruction of forest roads because of unplanned and disorganized design causes forestry activities to not be carried out in a healthy way and causes many environmental problems that affect social life and nature. Landslide disaster, which has a significantly more destructive effect in the region compared to other disaster types, has become one of the most important factors to be considered during the design and building of forest roads. Therefore, considering the LSMs of the region to produce forest road routes makes it possible for the forest roads to be healthy and long-lasting.

The objective of this study is to determine alternative forest roads using the produced LSMs. To achieve this goal, firstly, LSMs of Tonya district were produced using FR and MIV methods and the performances of these methods were compared. In addition, unlike the previous scientific studies focused on developing LSM, this work investigated the landslide risk associated with the forest roads currently under the responsibility of the forest regional directorate. Lastly, this research is to create new routes for the forest road using costpath analysis. These routes will then be compared with the existing roads. This study offers an exemplary approach to developing optimal alternative routes for forest road in landslide-prone areas. By designing forest road routes while considering LSM, it will be possible to prevention potential natural disasters caused by landslides in the future and support the successful implementation of forestry policies in a sustainable manner.

2. Method

2.1. Study area

Based on the report compiled from extensive research conducted by the Provincial Disaster and Emergency Directorate, Trabzon province in Türkiye has experienced the highest number of landslides among all other provinces, with a total of 1673 occurring between 1950 and 2019. In addition, considering the count of landslides that occurred in 2019, Trabzon ranks first with 102 landslides [66]. The most recent statistical data regarding landslide disasters at the provincial level is based on the year 2019.

In this study, the town of Tonya in the Trabzon province was selected as the study area (Figure 1). The Tonya district, located within Trabzon, stands out as one of the prominent districts in terms of the frequency of landslide incidents and the number of people affected by these disasters. The study area contains very steep regions in terms of topography. Additionally, since the annual average precipitation value in the region is approximately 2200 mm, it has been observed that the region has a very high tendency towards landslide and rockfall disasters. When examining the lithological structure of the research area, it has been noted that the region mostly consists of volcanic and volcano-clastic units [67].

The altitude values of Tonya district, characterized by its steep terrain, range between 250 and 2350 m, with slope values varying between 0° to 80°.

According to the 2020 data for Tonya district, which covers an area of 264 km², the population density is 13914. The region experiences a transitional climate, combining the characteristics of the Black Sea climate and continental climate. During the summer months, the temperature in the area reaches around 20°C, while in the winter months; it drops to approximately 6-7°C [68].

2.2. Workflow

The process steps applied in this study were converted into a workflow chart as depicted in (Figure 2).

Figure 2 summarizes the methodology in the article. The geological and geomorphological factors used in the production of the landslide susceptibility map and the landslide inventory map of the study area constitute the data production part of this study. The landslide inventory map is randomly divided into training (70%) and validation (30%) data. The production of landslide susceptibility maps of the study area using two different models constitutes the second stage of the study. Then, the verification phase of the landslide susceptibility maps produced was started. At this stage, the verification of the maps was carried out with the help of verification data randomly derived from the landslide inventory map. Then, the risk status of existing forest roads was examined using validated landslide susceptibility maps. Finally, alternative forest road routes were produced on the base map created by combining landslide susceptibility maps.
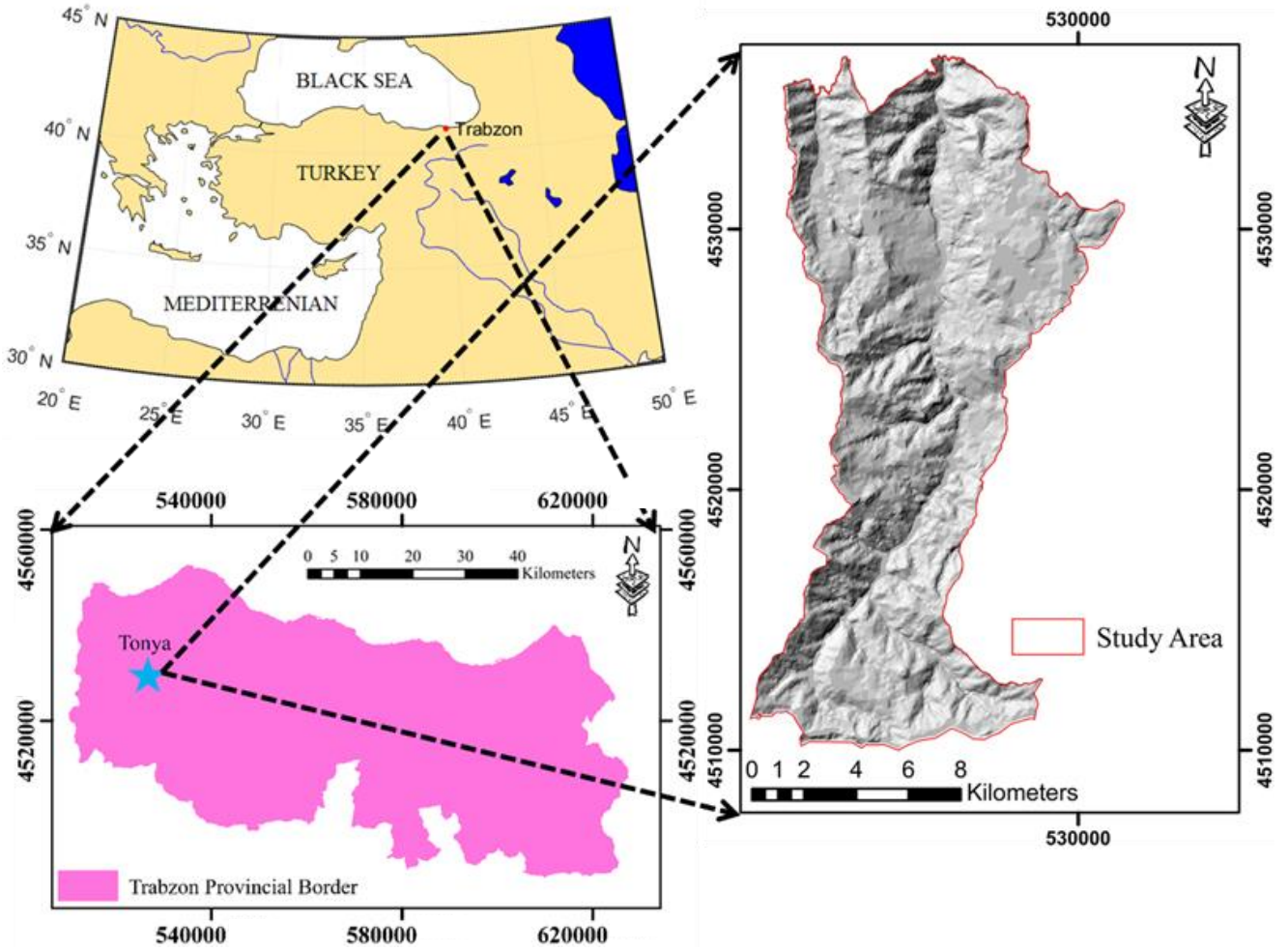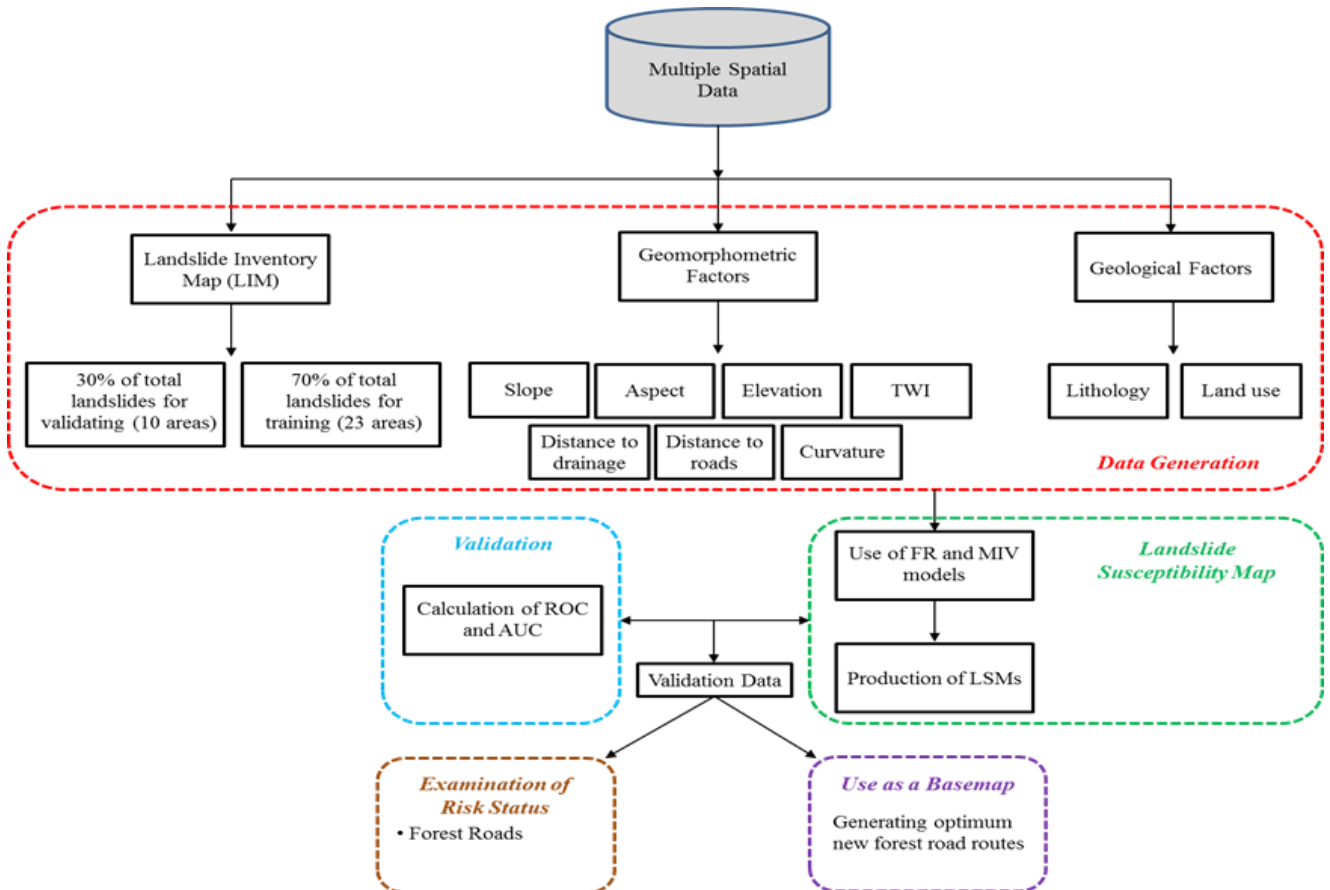
Figure 1. Study area.

Figure 2. Workflow.

2.3. Factors used in the production of LSM

LSM is a type of map that illustrates the tendency of areas in a region for landslide disaster, divided into various classes. Type of map is generated based on the correlations between the landslide inventory map (LIM) and the factors that trigger the landslide [28, 35].

The production of a LSM is primarily based on the availability of a LIM. An LIM serves as a foundational map created for a specific region and at a particular scale. This map encompasses spatial data related to landslide disasters that have occurred in a region from the past to the present. The spatial information in the map includes details about the position and magnitude of the landslide events [16]. The precise and reliable generation of an LIM significantly influences the accuracy of all derived products from it. Therefore, it is crucial to establish a well-designed LIM specifically tailored for the area to achieve high level of correctness in the LSM.

In this study, the utilized LIM was created through the digitization of reports obtained from comprehensive area surveys conducted by the General Directorate of Mineral Research and Exploration. As a result, the produced LIM for the study area encompasses 33 distinct landslide zones, covering a total surface area of 15.68 km² (Figure 3).

Within the context of this application, the generated LIM is categorized into two distinct groups: training data and validation data. In this context, 23 landslide areas were arbitrarily determined as training data (70%) and 10 landslide areas as validation data (30%) (Figure 3).
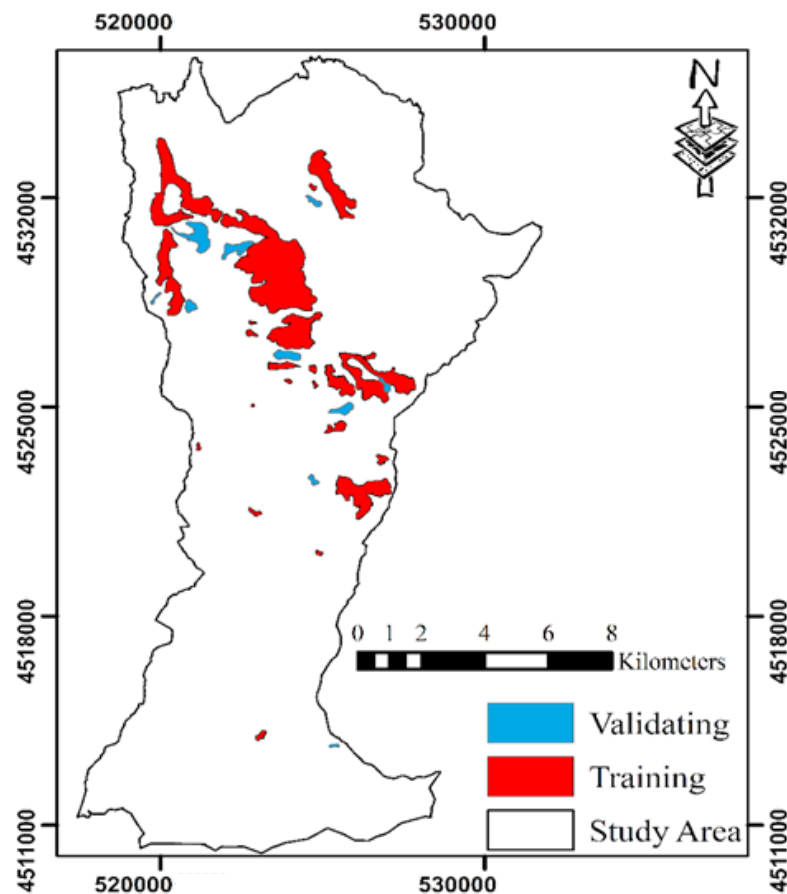

Figure 3. LIM for the study area.

The selection of the factors used in the production of the LSM is a significant research topic that directly affects the applicability and realism of the LSM. Since the parameters that trigger the landslide vary from region to region, the morphological, physical, geological, and meteorological characteristics of that region should be considered in the production of a LSM for a region [7].

In this study, nine main factors triggering landslide have been identified. These factors include slope, aspect, elevation, lithology, land use, distance to road, distance to drainage, curvature, and topographic wetness index (TWI).

It is expected that the factors used in the LSM produced with the help of statistical-based models are independent of each other and therefore the correlations between them are weak [36]. Two main indices used in the determining this correlation are, Tolerance (TOL) and variance inflation factor (VIF), which are frequently employed in the scientific researches. If the TOL value exceeds 0.1 or the VIF value is below 10, it signifies that the factors employed in generation the LSM are mutually independent, indicating a lack of significant correlation among them [69, 70]. The TOL and VIF values of the factors employed in this research were obtained with the help of the R software, which is one of the statistical-based software (Table 1). When the calculated TOL and VIF values of all factors were considered, it was observed that there was no strong relationship among the factors.

Table 1. Indicative values of factors.

Factors	VIF	TOL
Slope	1.5406	0.6491
Aspect	1.0527	0.9499
Elevation	1.4720	0.6793
Land Use	1.1828	0.8455
Lithology	1.0206	0.9798
TWI	1.3261	0.7541
Curvature	1.1203	0.8926
Distance to drainage	1.1105	0.9005
Distance to roads	1.4928	0.6699

In this research, the factors employed in generating the LSM were prepared by utilizing a map with a scale of 1: 25,000 and a contour interval 10 meters. This process was carried out through Topo to Raster analysis in the ArcGIS program and a high-resolution digital elevation model (DEM) with a resolution of 10 m x 10 m was created. Consequently, slope, aspect, elevation, TWI, and distance to drainage, which are utilized in the generation of the LSM, were created employing the DEM data through the utilization of ArcGIS software.

Slope is considered one of the most important factors that can affect landslide disaster. Many scientific articles in the literature support the view that increasing the slope angle increases the susceptibility to landslide [71, 72]. Slope, which is frequently used in the production of susceptibility maps, has been preferred as the main factor in many scientific studies produced today [29, 36, 73, 74]. The slope factor produced for this study is divided into a total of 10 subclasses at 5° intervals (Figure 4c). Aspect is another important factor used in the production of LSMs. This type of disaster occurs on slopes with a certain orientation. Sunlight, drainage, and climatic effects of the regions facing different aspects of the land include differences. Therefore, the tendency levels towards landslide disasters of regions with different aspect values are also different [75]. The aspect produced for the research area is separated into 9 different groups in total (Figure 4a). Elevation is another important factor used in the production of a LSM. The elevation value of a region is an important criterion that directly affects the gravitational potential energy in that region [76]. In this study, the elevation factor used in the production of the LSM was divided into a total of 10 subclasses (Figure 4b). Lithology is another factor used in this study. The types of materials in the existing layers under the ground have different properties and types of movement from each other. Since the sliding movements and water permeability resistances of each material structure are different from each other, their effects on slope stability are also different [77]. The lithology map used was created using ArcGIS software, utilizing the geological map created at a scale of 1:25000 (Figure 4d). In the lithology map generated for the study area, there are 9 different soil types (Kru1, Kru2, Kru3, Kru4b, Kru5b, Kru5a, Gama2, Jlh, Ev). The outcropping units of the study area mostly consist of volcanic and volcano-clastic units. The age of these units fallows a sequence from the Jurassic to the Late Cretaceous and ends with the Eocene. There are Eocene aged, units expressed as Ev consisting of basalt, andesite and pyroclasts and containing partly sandy limestone, and Gama2 units with

granite, granodiorite, quartz diorite and dolerite structures. While Kru1, Kru2, Kru3, Kru4b, Kru5a, basalt, andesite, dacite, rhyodacite and pyroclasts from Late Cretaceous units, Kru5b has sandy reef limestone content. When the spatial dispersion of these units in the research area is analyzed, it becomes apparent that the Ev units have the highest frequency, comprising approximately 35% of the total. Curvature is another basic terrain factor used in the production of a LSM. This type of factor, defined as the slope angle or the amount of change in aspect, is divided into 3 classes: concave, flat and convex [77]. The factor in question was created using ArcGIS software with the DEM (Figure 4g). Land use is another factor commonly utilized in LSMs. Land use is a type of map in which land and soil are classified according to their capabilities, taking into account climatic characteristics. In this type of map, based on basic soil surveys, the soil is divided into eight classes. The first four classes include lands with land structure suitable for agriculture. On the other hand, the last four classes include the classes where there are pastures, forests and lands suitable for natural life, which are not suitable for agriculture. The first four and the last four classes are ordered according to their profile shape and slope level. Within the study area, four classes (I, IV, VI, and VII) have been identified (Figure 4f). The topographic wetness index (TWI) is an additional factor that measures the influence of water movement and accumulation on the terrain across the basin [78]. The TWI is commonly employed to assess the influence on hydrological processes. Calculation of this index is achieved through Equation 1.

$$TWI = \ln \frac{a}{\tan\beta} \qquad (1)$$

Where a value represents the upward slope area at the unit point, and the $\tan\beta$ value represents the slope angle at the point. This factor, which was produced using ArcGIS software with the help of DEM, was divided into 5 subclasses in total in this study (Figure 4e). Another factor generated from the DEM is the distance to the drainage. This factor was generated using the hydrological analysis module, which is one of the spatial research tools provided in the ArcGIS software. The factor to drainage network was computed for the research area and separated into 10 subclasses. The maximum distance to the drainage network was determined as 2260 m (Figure 4h). The distance to the road factor is another important aspect considered in this study. The road network, often characterized by unplanned and haphazard construction, significantly influences the slope stability in the region. The road network was obtained from Open Street Map data and 1:25,000 scale maps. Once the road network was established, the process of creating the distance map to the road network commenced. The ArcGIS software was employed to determine the distance from every pixel to the road network. The distance to the road factor was separated into 10 subclasses (Figure 4i). Using the ArcGIS software, all factors employed in the production phases of the LSM were converted into raster, ensuring a spatial resolution of 10 m.

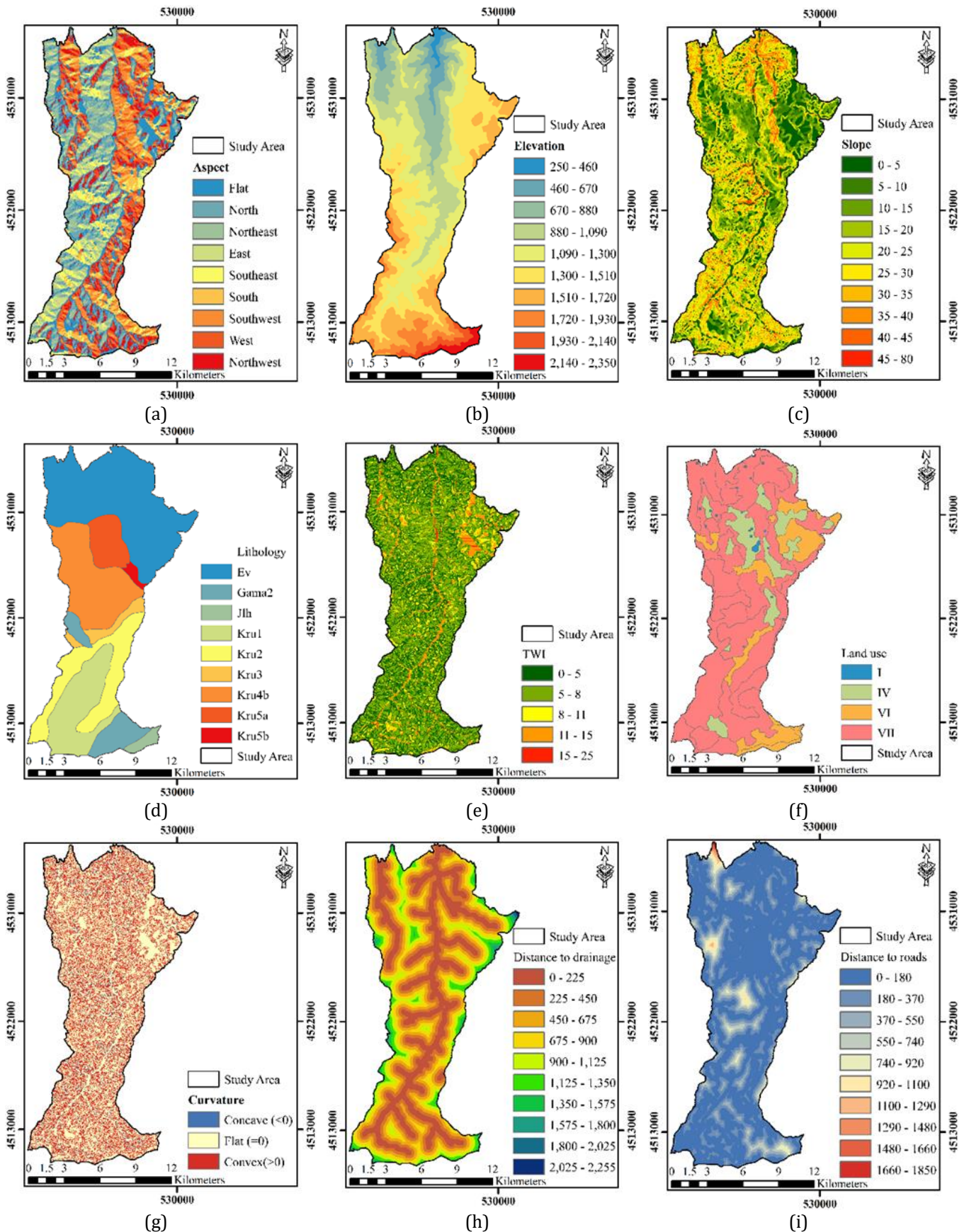**Figure 4.** Factors used in LSM (a: aspect, b: elevation, c: slope, d: lithology, e: TWI, f: land use, g: curvature, h: distance to drainage, i: distance to road).

2.4. Models used in the production of LSM

Two different models, FR and MIV, were used in the production of LSMs of the study area.

2.4.1. FR model

Various approaches exist for predicting future landslides. The FR model employs a methodology that

seeks to establish a correlation between the factors influencing past landslides and those that may take place in times to come. The primary objective of the FR model is to estimate potential landslides by analyzing the factors that have triggered previous occurrences of landslides. By employing this approach, it becomes possible to gain a comprehensive understanding of the relationship among old landslide data and the probability of future landslide occurrences [28, 54, 55]. The FR model, which is one of the statistical-based approaches, has a simpler and more understandable structure compared to others. Moreover, the FR model is a reliable model type that is frequently used in the production of LSMs that require high accuracy and precision. For this reason, the FR model has been used in numerous scientific researches to produce LSMs. In this study, each of the factors affecting the landslide is divided into various subclasses. FR model values of each class were calculated with Equation 2.

$$F_r = \frac{\frac{N_{pix}(L_{ij})}{N_{pix}(L)}}{\frac{N_{pix}(S_{ij})}{N_{pix}(S_a)}} \qquad (2)$$

In this context, $N_{pix}(L_{ij})$ signifies the count of pixels located within the landslide area belonging to the jth subclass of factor i, $N_{pix}(L)$ the all count of pixels within all landslide areas in the study area, and $N_{pix}(S_{ij})$ denotes the corresponding count of pixels. And finally, $N_{pix}(S_a)$ represents the all count of pixels.

Factors with FR values higher than 1 are known to have better correlations with landslide areas than factors with FR values lower than 1 [28]. The sum of the FR values of each subclass is equal to the landslide susceptibility index (*LSI*). Equation 3 is used to calculate this index value.

$$LSI = \sum_{i=1}^{n} Fr_i = Fr_1 + Fr_2 + Fr_3 + \cdots + Fr_n \qquad (3)$$

A high index value means that the region has a high tendency to landslide disaster. The *LSI* values calculated for the study area change among 3.00 and 14.11 (Table 2).

The FR model was utilized to create the LSM. The map was separated into 5 groups in total, considering the risk situation (Figure 5).

2.4.2. MIV model

One of the other statistical-based models frequently used in the literature is the MIV model. The MIV model is a type of model that is depend on information theory and works in accordance with a statistical data analysis method [79].

This model has an approach that considers the information values of the factors used in the production of the LSM. In this context, the information values of the subclasses of whole the factors used in the production of the sensitivity map were calculated with Equation 4.

$$I(H, x_j) = ln \frac{\frac{N_{pix}(S_j)}{N_{pix}(N_j)}}{\frac{\sum N_{pix}(S_j)}{\sum N_{pix}(N_j)}} \qquad (4)$$

Where, $N_{pix}(S_j)$ value symbolizes the total count of pixels falling on landslide areas in subclass j of all factors, and $N_{pix}(N_j)$ value represents the all count of pixels in subclass i of factors. In addition, the $\sum N_{pix}(S_j)$ value symbolizes the whole number of pixels falling on the landslide areas, and the $\sum N_{pix}(N_j)$ value symbolizes the all pixel area in the study area.

The $I(H, x_j)$ value calculated because of the equation numbered 3 symbolizes the information value in the j subclass of the factors.

The cumulative sum of the information values computed for the subclasses of all factors, as determined by Equation 4, equals the *LSI*. The specific formula is provided in Equation 5.

$$LSI = \sum_{j=1}^{n} I(H, x_j) \qquad (5)$$

A negative value of *LSI* means that likelihood of a landslide disaster to occur in the relevant region is low. A *LSI* value of zero indicates that the likelihood of a landslide disaster happening is average or moderate. Finally, a positive value of *LSI* means that the probability of a landslide disaster is above medium.

The MIV for each subclass of the nine factors was determined by utilizing the landslide data from the training set and referring to the LIM (Table 2). The results obtained from the MIV model revealed a range of *LSI* values between 2.91 and 9.67.

The LSM produced using MIV was separated into 5 different groups in total, considering the risk situation (Figure 6).

3. Results

In line with the data obtained in Table 2, LSMs were generated employing both the FR and the MIV (Figure 5-6). Each of the LSMs produced on different models is separated into 5 groups.

The spatial and percentile distributions of the LSM produced using FR are 804.52 ha (4%), 1206.78 ha (6%), 1206.78 ha (6%), 6637.29 ha (33%), and 10,257.63 ha (51%) (very high, high, medium, low and very low). The areal and percentage distributions of the LSM produced using MIV were calculated as 1206.78 ha (6%), 1810.17 ha (9%), 4223.73 ha (21%), 6033.90 ha (30%) and 6838.42 ha (34%). In light of these results, the areal and percentage distribution of high and very high classes in the LSMs created from the FR and MIV models are seen as 2011.30 ha (10%) and 3016.95 ha (15%), respectively (Figure 7).

Table 2. The FR and MIV values were calculated for the various factors.

| Factors	Subclasses	No. of pixels in domain	Percentage of domain	No. of landslide pixels	Percentage of landslide	FR	MIV
Elevation	250-460	15,931	0.7958	381	0.2430	0.3054	0.3487
	460-670	69,396	3.4666	8702	5.5510	1.6013	1.6421
	670-880	202,706	10.1260	50,971	32.5143	3.2110	2.7893
	880-1090	352,580	17.6129	60,449	38.5603	2.1893	1.9431
	1090-1300	433,825	21.6714	27,395	17.4752	0.8064	0.9677
	1300-1510	459,035	22.9308	8211	5.2378	0.2284	0.3185
	1510-1720	297,923	14.8825	656	0.4185	0.0281	0.0590
	1720-1930	103,898	5.1902	0	0.0000	0.0000	0.0000
	1930-2140	40,919	2.0441	0	0.0000	0.0000	0.0000
	2140-2350	25,617	1.2797	0	0.0000	0.0000	0.0000
Slope	0-5	335,526	16.7610	22,208	14.1664	0.8452	0.9674
	5-10	104,899	5.2402	24,963	15.9238	3.0388	2.4013
	10-15	242,180	12.0979	54,410	34.7080	2.8689	1.9788
	15-20	301,487	15.0606	29,424	18.7695	1.2463	1.0370
	20-25	328,485	16.4092	13,262	8.4598	0.5156	0.7055
	25-30	305,965	15.2843	6219	3.9671	0.2596	0.4021
	30-35	213,039	10.6422	3668	2.3398	0.2199	0.2711
	35-40	110,780	5.5339	1709	1.0902	0.1970	0.3164
	40-45	41,041	2.0502	533	0.3400	0.1658	0.2253
	45-80	18,428	0.9206	369	0.2354	0.2557	0.2984
Aspect	Flat	390,321	19.4982	29,351	18.7229	0.9602	1.3092
	North	225,785	11.2789	33,997	21.6866	1.9228	1.5017
	Northeast	230,546	11.5168	30,017	19.1478	1.6626	1.2963
	East	176,522	8.8180	6232	3.9754	0.4508	0.8721
	Southeast	123,494	6.1691	1678	1.0704	0.1735	0.2673
	South	159,427	7.9641	1494	0.9530	0.1197	0.1933
	Southwest	240,937	12.0358	10,537	6.7215	0.5585	0.7042
	West	230,714	11.5252	20,146	12.8511	1.1150	1.0853
	Northwest	224,084	11.1940	23,313	14.8713	1.3285	1.1928
Curvature	<0	723,592	36.1465	57,730	36.8258	1.0188	0.9239
	0	542,316	27.0910	43,149	27.5246	1.0160	0.9410
	>0	735,922	36.7625	55,886	35.6495	0.9697	1.0498
TWI	0-5	579,624	28.9547	26,271	16.7582	0.5788	0.6214
	5-8	1,023,829	51.1447	96,262	61.4053	1.2006	1.0986
	8-11	214,909	10.7356	20,985	13.3863	1.2469	1.1849
	11-15	163,126	8.1488	11,280	7.1955	0.8830	0.9321
	15-25	20,342	1.0162	1967	1.2547	1.2348	1.1244
Lithology	Ev	729,115	36.4323	59,097	37.6978	1.0347	0.9572
	Gama2	120,665	6.0294	273	0.1741	0.0289	0.0897
	Jlh	27,885	1.3934	0	0.0000	0.0000	0.0000
	Kru1	284,953	14.2385	0	0.0000	0.0000	0.0000
	Kru2	272,579	13.6202	9175	5.8527	0.4297	0.5034
	Kru3	54,295	2.7130	3794	2.4202	0.8921	0.9593
	Kru4b	370,184	18.4973	20,575	13.1247	0.7095	0.7682
	Kru5a	124,283	6.2102	56,822	36.2466	5.8367	3.2799
	Kru5b	17,327	0.8658	7029	4.4838	5.1788	3.1080
Distance to Drainage (m)	0-225	494,398	24.5745	43,222	27.5712	1.1219	1.0672
	225-450	432,259	21.4859	32,462	20.7074	0.9638	1.1230
	450-675	393,813	19.5749	29,953	19.1069	0.9761	1.0566
	675-900	320,570	15.9342	24,903	15.8856	0.9969	1.0834
	900-1125	216,948	10.7836	17,905	11.4216	1.0592	0.8937
	1125-1350	105,726	5.2552	6952	4.4347	0.8439	1.1028
	1350-1575	35,604	1.7697	1349	0.8605	0.4862	0.6217
	1575-1800	9789	0.4866	19	0.0121	0.0249	0.1470
	1800-2025	1741	0.0865	0	0.0000	0.0000	0.0000
	2025-2265	982	0.0488	0	0.0000	0.0000	0.0000
Distance to Roads (m)	0-180	1,314,001	65.3137	13,2982	84.8289	1.2988	1.1834
	180-360	406,420	20.2015	14,669	9.3573	0.4632	0.6217
	360-530	169,054	8.4030	4500	2.8705	0.3416	0.3922
	530-710	75,094	3.7326	1704	1.0870	0.2912	0.3758
	710-880	30,522	1.5171	1534	0.9785	0.6450	0.7004
	880-1060	10,250	0.5095	792	0.5052	0.9916	1.1028
	1060-1240	3167	0.1574	584	0.3725	2.3665	2.0793
	1240-1410	1457	0.0724	0	0.0000	0.0000	0.0000
	1410-1590	1311	0.0652	0	0.0000	0.0000	0.0000
	1590-1770	554	0.0275	0	0.0000	0.0000	0.0000
Land Use	I	9938	0.4940	3214	2.0502	4.1504	2.7814
	IV	235,784	11.7199	126,479	80.6806	6.8841	3.1447
	VI	276,189	13.7282	12,197	7.7804	0.5667	0.6879
	VII	1,489,919	74.0579	14,875	9.4887	0.1281	0.2019
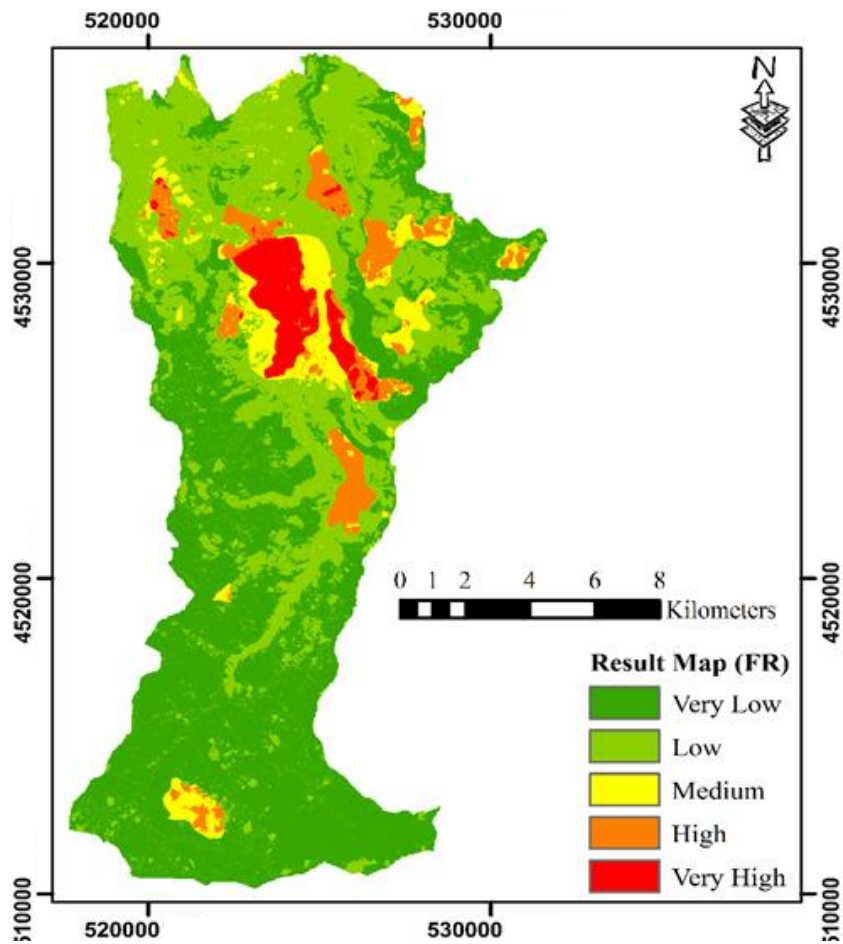
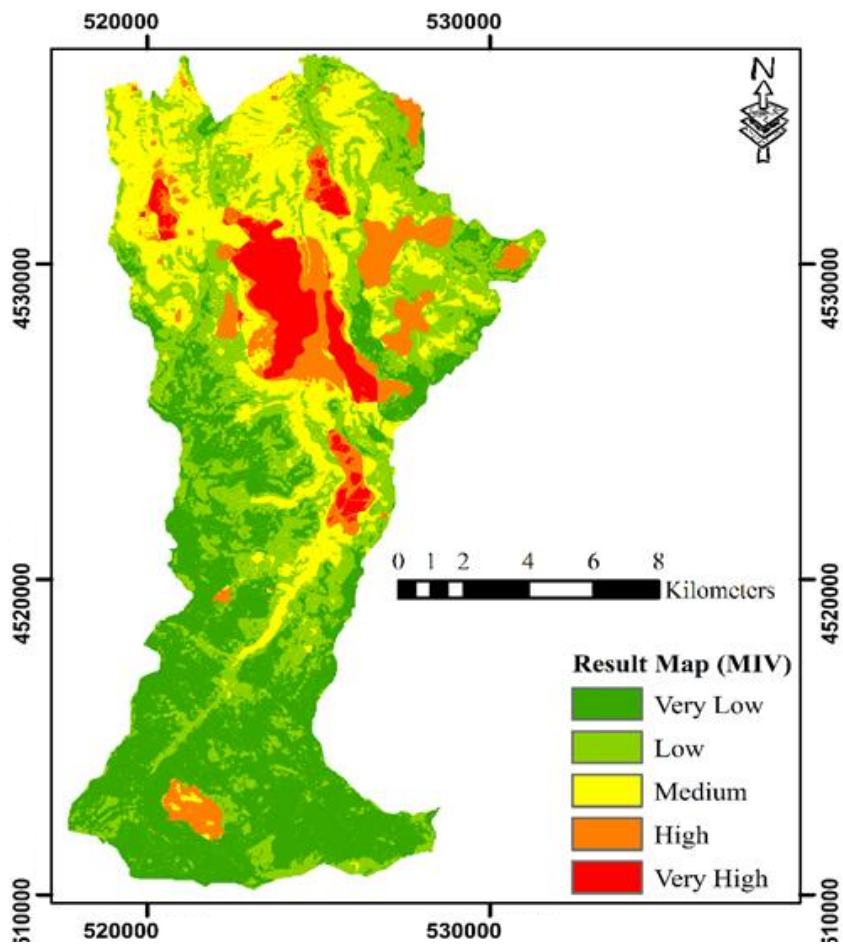**Figure 5.** LSM generated by the FR model.

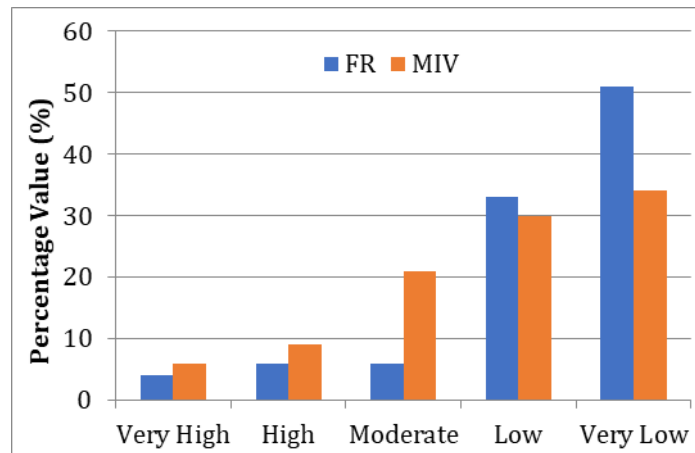**Figure 6.** LSM generated by the MIV model.

Figure 7. Percentage distributions of classes in the LSM for FR and MIV models.

3.1. Validation of LSMs

The accuracy of the generated LSM is a very important criterion in terms of the applicability and realism of the map. Therefore, testing the correctness of the generated LSM is a clear indication of how reliable the product produced is.

There are many methods to check the accuracy of the LSM produced today. The receiver operating characteristic (ROC) curve and the area under the ROC curve (AUC) are widely employed and highly reliable techniques in the researches [18, 35, 80, 81]. In this context, the precision of the generated LSM was evaluated employing the ROC and AUC methods. The ROC curve consists of two axes (horizontal and vertical). The X-axis is the false positive rate, while the Y-axis is the true positive rate. The most basic criterion used in the analysis of the correctness of the LSM produced in this curve is the AUC value. A model with values between 0.5 and 1 AUC is defined as a model type that is adequate in terms of accuracy [18].

The accuracy of the LSMs generated employing the FR and MIV models was evaluated employing the success rate and prediction rate methods. The AUC values of the FR and MIV models were computed employing the training data from the LIM, as part of the success rate analysis.

The LSMs obtained from both models were overlapped with the training data and the degree of overlap of the layers was checked. Thus, the success rate percentages of both models were calculated. In this study, the success rates of the FR and MIV models were computed as 82.1% and 83.4%, respectively (Figure 8). Prediction rate method, on the other hand, is a type of method that is frequently used in estimating areas that are prone to landslide according to the success rate method. This type of method aims to test how accurately the produced LSMs identifies areas prone to landslides [28, 82]. The validation dataset, which constitutes 30% of the LIM and includes ten randomly determined landslide areas, was used to estimate the areas prone to landslides. In this context, the AUC values for the FR and MIV models are 79.7% and 80.9%, respectively (Figure 9). As a result, although the MIV model was more successful than the FR model in detecting areas prone to landslides, it was observed that both models gave very good results in this study.
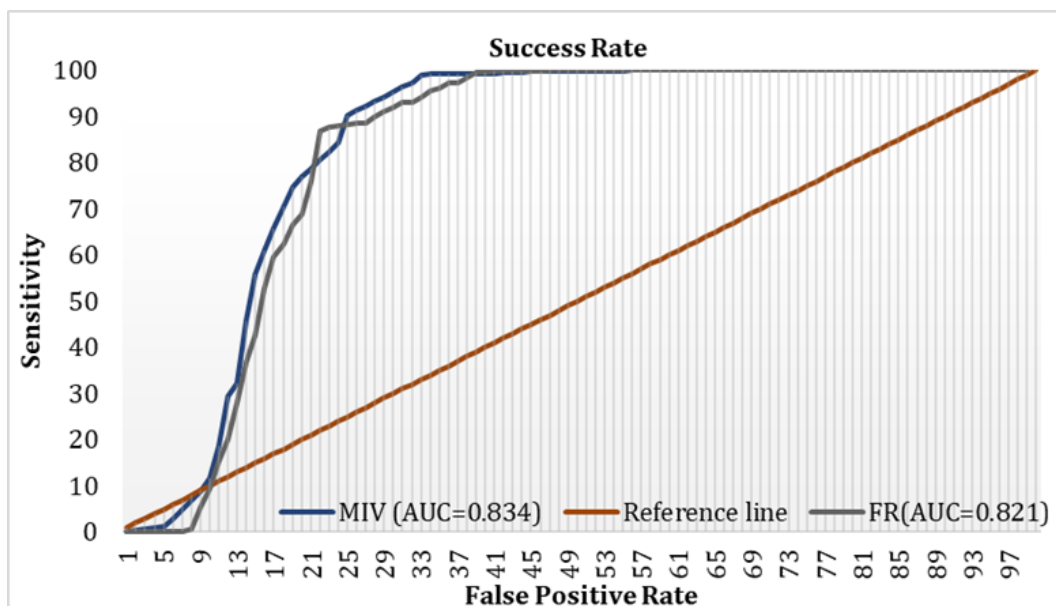

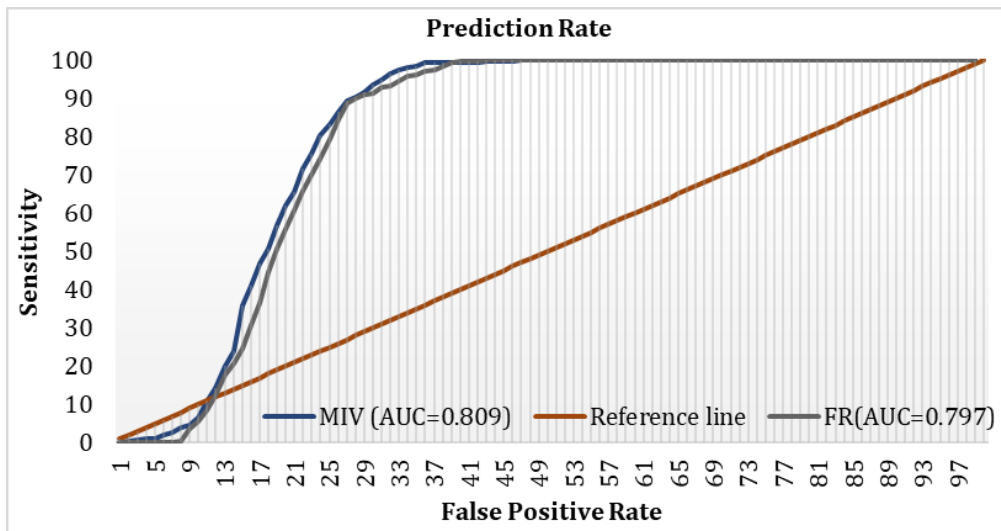**Figure 8.** Success rate curves for FR and MIV models.

Figure 9. Curves displaying the prediction rates for the FR and MIV models.

3.2. Risk situations of forest roads and determination of new routes

This section investigates the risk conditions of forest roads in the study area by employing LSMs generated through the utilization of FR and MIV models. Within the study area, there are approximately 125 km of forest roads present (Figure 10).

In this context, forest roads overlapped with LSMs produced on two different models (Figure 11). The risk situations on the LSMs of forest roads were evaluated by dividing them into 4 classes. Considering the LSM produced on the FR model, it was determined that 9.5 km (7.6%) of the 125 km forest road is on high and very high-risk areas. In the LSM created using the MIV model, this value is 11.85 km (9.5%).
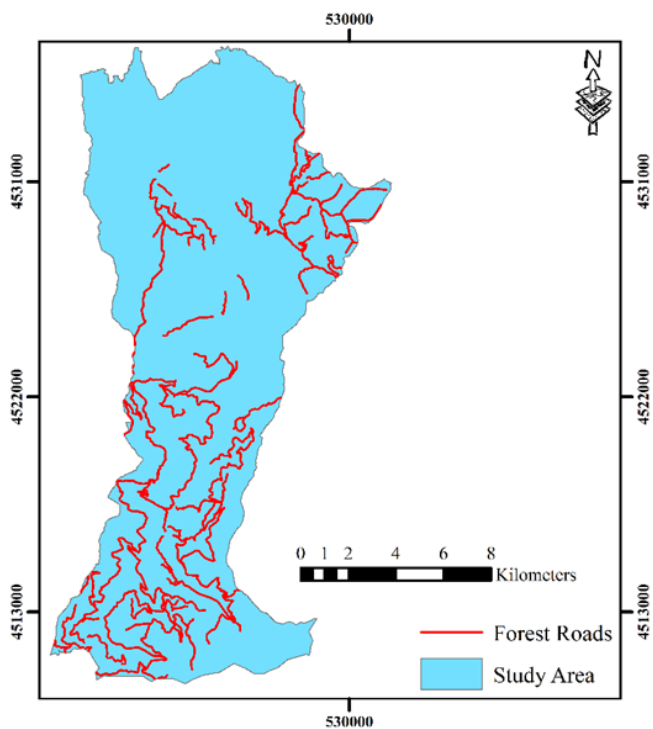

Figure 10. Available forest roads in the study area.

The forest roads, which are in the risky classes in the

LSMs produced through both models, pose a risk in terms of the healthy execution of the forestry policies implemented by the forest enterprises in that region. Therefore, it is significant for the continuity of forestry activities to be able to produce alternative forest road routes instead of the risky forest roads. In the process of generating alternative forest road routes, a single map derived from the combination of 2 different LSMs produced with the help of different models in this study was used as a base map. A single map derivation from two different LSMs produced on different models for the same region was performed with the overlap analysis in ArcGIS software (Figure 12).

The risk situations of the available forest roads area were determined by considering the high and very high classes in the combined LSM shown in Figure 12. The lengths of the existing forest roads in both classes are given in Table 3. In addition, in the light of the evaluations made on the combined LSM, it has been determined that 5.4 km of the 125 km forest roads are in the very high (4.28%) class and 5.3 km in the high (4.27%) class. Therefore, it has been observed that forest roads with a length of 10.68 km in regions with high and very high landslide risk carry a high risk in terms of landslides.

It is necessary to produce new alternative forest road routes in order not to interrupt the forestry activities in the region, instead of the canceled forest road routes in regions with high and very high landslide risk. To achieve this objective, costpath analysis was performed utilizing the ArcGIS software. Costpath analysis is a type of analysis that aims to determine the most suitable route in terms of cost, considering criteria such as slope, mandatory point, restricted area. In this study, the base map produced because of overlaying the LSM combined with the slope map was used as an input for costpath analysis. The new forest road routes obtained because of the costpath analysis are presented in Figure 13. In addition, the quantity information regarding the new forest road routes in question are given in Table 4. In this study, 10.68 km of forest roads in the study area were canceled due to being on risky landslide areas, while new forest road routes of 5.77 km were produced with the help of costpath analysis in the GIS.
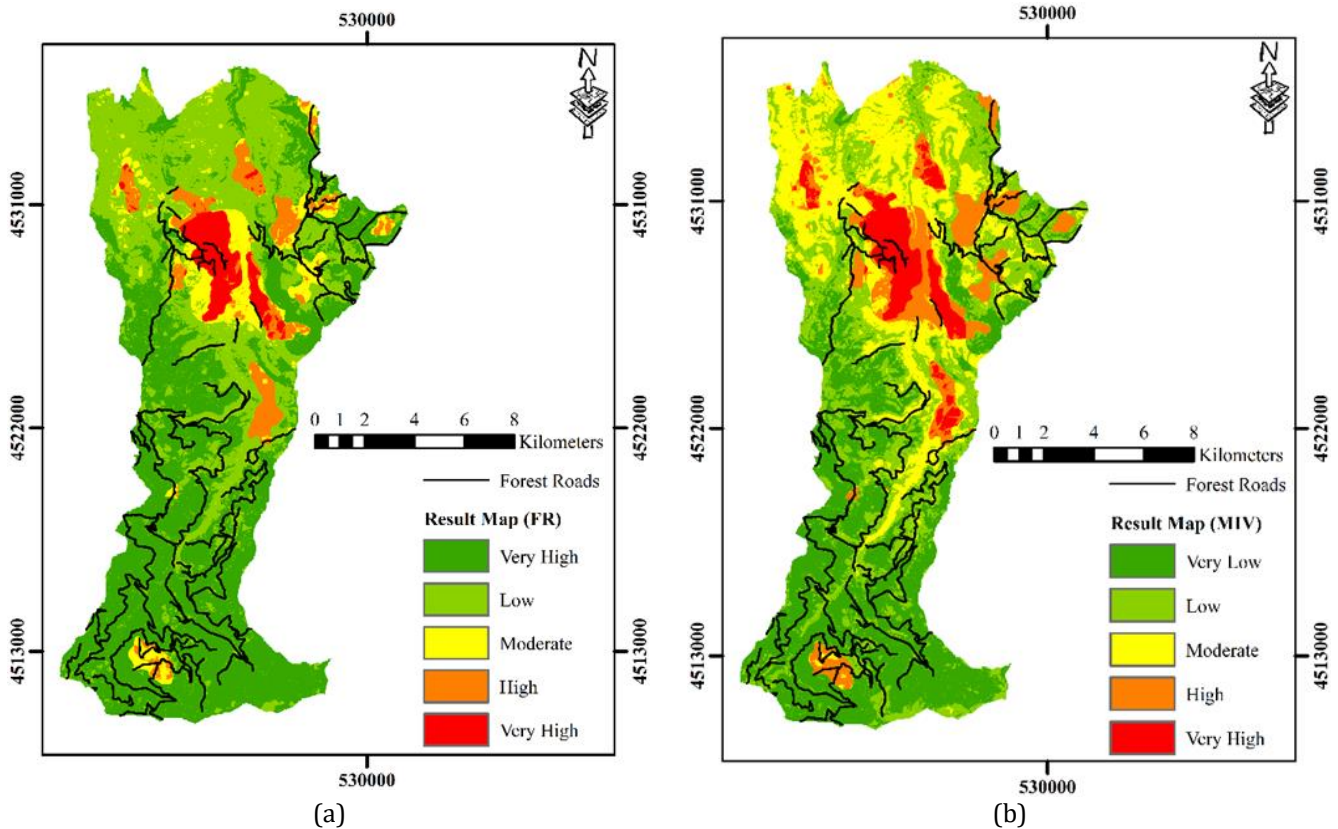
(a)   (b)

Figure 11. Representation of forest roads on produced LSMs (a: FR model, b: MIV model).

Table 3. Forest roads in high and very high classes, canceled routes.

Forest road number	Forest road intersection with risk classes (m)		Canceled route (m)
	Very High	High	
1	-	344.35	344.35
2	-	1128.34	1128.34
3	-	176.56	176.56
4	-	111.80	111.80
5	-	415.15	415.15
6	-	322.92	322.92
7	187.78	22.91	210.69
8	1590.82	-	1590.82
9	150.64	-	150.64
10	595.98	-	595.98
11	964.14	-	964.14
12	442.24	-	442.24
13	438.12	-	438.12
14	981.72	-	981.72
15	-	159.16	159.16
16	-	227.7	227.7
17	-	185.56	185.56
18	-	595.01	595.01
19	-	241.82	241.82
20	-	608.23	608.23
21	-	794.63	794.63
Total	5351.44	5334.14	10685.58

4. Discussion

The LSM for the study area was initially produced by [67]. The author aimed to create an LSM for the region using a method falling, within the cluster classifier category known as fuzzy adaptive resonance theory (FuzzyART-BURT). The production of the LSM involved, lithology, elevation, slope, aspect, stream power index and TWI data. The accuracy of the LSM resulting from the

study was assessed with the area under the curve (ROC-EAA) method. Following the validation analysis, the AUC value was calculated as 0.72, indicating the success of the generated LSM.
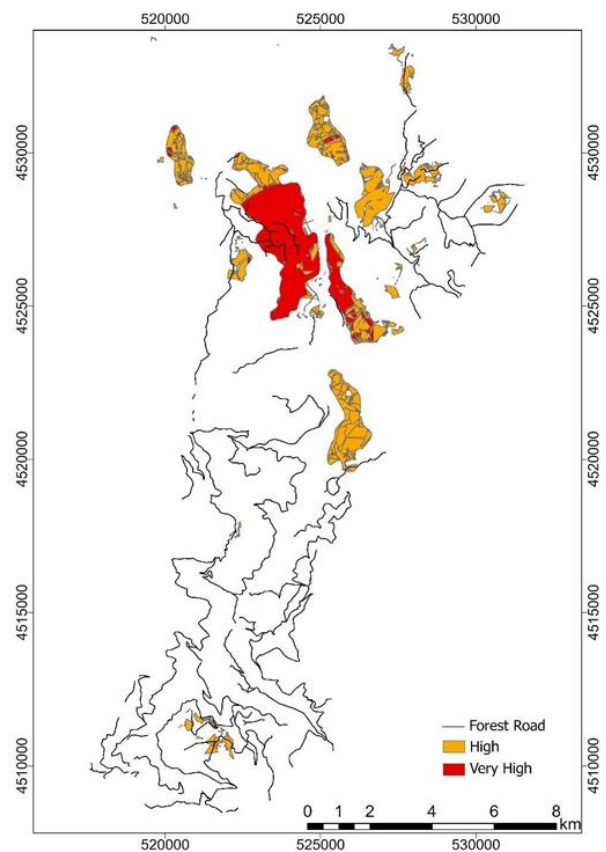

Figure 12. Base map obtained by overlaying the LSMs produced on the FR and MIV models.

To validate the produced LSMs, ROC and AUC parameters were employed, comparing the performance of the FR and MIV models using ROC curves and AUC analysis. According to many scientific studies, a model with AUC values between 0.5 and 1 is considered adequate in terms of accuracy [18]. The computed AUC values for the success rate of the FR and MIV models were 82.1% and 83.4%, respectively. Additionally, the AUC values for the predicted rate were determined as 79.7% and 80.9% for the FR and MIV models, respectively. As a result, although the MIV model outperformed the FR model in detecting areas prone to landslides, both models yielded excellent results.

Table 4. New forest road routes generated with costpath analysis.

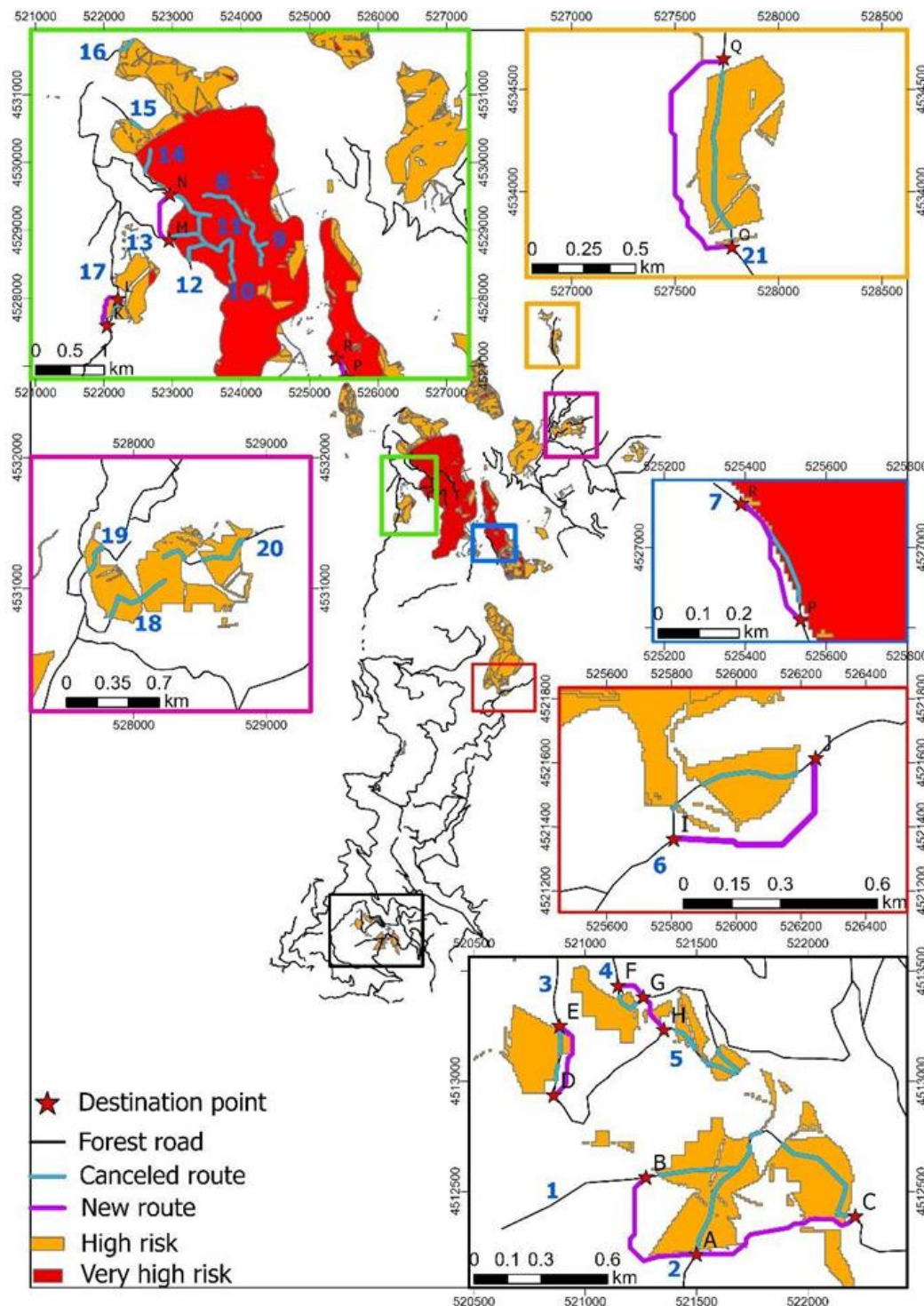| New route name	New route distance (m)
A-B	673.84
A-C	797.69
D-E	375.16
F-G	319.79
I-J	648.36
P-R	254.80
K-L	614.65
M-N	819.08
O-Q	1262.99
Total	5766.36

Figure 13. New forest road routes map.

5. Conclusion

LSMs of the research were generated for the research area using two different models, namely FR and MIV (Figure 5-6). Given the both models are statistically based, it has been frequently emphasized in the literature that the maps created from these models are more understandable [32, 52]. The LSMs were generated using nine factors (Figure 4) with the LIM serving as another input. There are 33 landslide areas recorded and processed on the LIM in study area (Figure 3). During the production of LSMs with the FR and MIV models, 70% of the landslide areas (23 landslide areas) were utilized for training the models, while the remaining 30% (10 landslide areas) were employed for model validation purposes. The random division of landslide areas into training and verification classes, was performed based on percentages referenced in the previous sentence using existing literature for both the distribution type and the percentages [83-87]. The second phase of the study involved assessing the risk conditions of existing forest roads based on the LSMs. In the LSMs generated with the help of FR and MIV models, it was determined that 7.6% and 9.5% of the existing forest roads are situated on areas with high and very high landslide risk. Producing new alternative forest road routes instead of existing forest roads in high and very high risk areas will facilitate forestry activities in that region. In the final stage of the study, a total of 9 alternative forest road routes were produced instead of existing routes affected by landslide (Figure 13) (Table 4). Costpath analysis in ArcGIS software was applied in the process of generating these alternative optimum forest road routes. This type of analysis frequently used in the literature, determines the optimum route between the start and end points [88-91]. As a result of the analysis, 10.68 km of existing forest roads in the study area were canceled due to their location in high risk landslide areas, while new forest road routes of 5.77 km were proposed. The newly determined routes play an important role in the healthy and systematic execution of forestry activities. For all that, the LSMs created with the two different models can serve as a base map for practitioners when the generating of new forest road routes or proposing alternative route solutions.

Author contributions

Fatih Kadı: Conceptualization, Methodology, Investigation, Data curation, Writing-Original draft preparation. **Osman Salih Yılmaz:** Writing-Original draft preparation, Software, Validation, Visualization, Reviewing and Editing.

Conflicts of interest

The authors declare no conflicts of interest.

References

1. Şentürk, E., & Erener, A. (2017). Determination of temporary shelter areas in natural disasters by GIS: A case study, Gölcük/Turkey. International Journal of Engineering and Geosciences, 2(3), 84-90. https://doi.org/10.26833/ijeg.317314

2. Kaya, H., & Gazioğlu, C. (2015). Real estate development at landslides. International Journal of Environment and Geoinformatics, 2(1), 62-71. https://doi.org/10.30897/ijegeo.302433

3. Stanley, T., & Kirschbaum, D. B. (2017). A heuristic approach to global landslide susceptibility mapping. Natural Hazards, 87, 145-164. https://doi.org/10.1007/s11069-017-2757-y

4. EM-DAT. (2023). The International Disaster Database. Inventorying hazards & disasters worldwide since 1988. https://www.emdat.be

5. Görüm, T., & Fidan, S. (2021). Spatiotemporal variations of fatal landslides in Turkey. Landslides, 18(5), 1691-1705. https://doi.org/10.1007/s10346-020-01580-7

6. Dahal, R. K., Hasegawa, S., Nonomura, A., Yamanaka, M., Masuda, T., & Nishino, K. (2008). GIS-based weights-of-evidence modelling of rainfall-induced landslides in small catchments for landslide susceptibility mapping. Environmental Geology, 54, 311-324. https://doi.org/10.1007/s00254-007-0818-3

7. Chen, W., Li, W., Hou, E., Zhao, Z., Deng, N., Bai, H., & Wang, D. (2014). Landslide susceptibility mapping based on GIS and information value model for the Chencang District of Baoji, China. Arabian Journal of Geosciences, 7(11), 4499-4511. https://doi.org/10.1007/s12517-014-1369-z

8. Ercanoglu, M., & Gokceoglu, C. (2004). Use of fuzzy relations to produce landslide susceptibility map of a landslide prone area (West Black Sea Region, Turkey). Engineering Geology, 75(3-4), 229-250. https://doi.org/10.1016/j.enggeo.2004.06.001

9. Komac, M., & Ribičič, M. (2006). Landslide susceptibility map of Slovenia at scale 1: 250,000. Geologija, 49(2), 295-309. https://doi.org/10.5474/geologija.2006.022

10. Petschko, H., Brenning, A., Bell, R., Goetz, J., & Glade, T. (2014). Assessing the quality of landslide susceptibility maps–case study Lower Austria. Natural Hazards and Earth System Sciences, 14(1), 95-118. https://doi.org/10.5194/nhess-14-95-2014

11. Chawla, A., Chawla, S., Pasupuleti, S., Rao, A. C. S., Sarkar, K., & Dwivedi, R. (2018). Landslide susceptibility mapping in darjeeling Himalayas, India. Advances in Civil Engineering, 2018(1), 6416492. https://doi.org/10.1155/2018/6416492

12. Silalahi, F. E. S., Pamela, Arifianti, Y., & Hidayat, F. (2019). Landslide susceptibility assessment using frequency ratio model in Bogor, West Java, Indonesia. Geoscience Letters, 6(1), 10. https://doi.org/10.1186/s40562-019-0140-4

13. Ram, P., Gupta, V., Devi, M., & Vishwakarma, N. (2020). Landslide susceptibility mapping using bivariate statistical method for the hilly township of Mussoorie

and its surrounding areas, Uttarakhand Himalaya. Journal of Earth System Science, 129, 1-18. https://doi.org/10.1007/s12040-020-01428-7

14. Sangeeta, Maheshwari, B. K., & Kanungo, D. P. (2020). GIS-based pre-and post-earthquake landslide susceptibility zonation with reference to 1999 Chamoli earthquake. Journal of Earth System Science, 129, 1-20. https://doi.org/10.1007/s12040-019-1319-y

15. Bahrami, Y., Hassani, H., & Maghsoudi, A. (2021). Landslide susceptibility mapping using AHP and fuzzy methods in the Gilan province, Iran. GeoJournal, 86, 1797-1816. https://doi.org/10.1007/s10708-020-10162-y

16. Kadi, F., Yildirim, F., & Saralioglu, E. (2021). Risk analysis of forest roads using landslide susceptibility maps and generation of the optimum forest road route: a case study in Macka, Turkey. Geocarto International, 36(14), 1612-1629. https://doi.org/10.1080/10106049.2019.1659424

17. Roccati, A., Paliaga, G., Luino, F., Faccini, F., & Turconi, L. (2021). GIS-based landslide susceptibility mapping for land use planning and risk assessment. Land, 10(2), 162. https://doi.org/10.3390/land10020162

18. Kincal, C., & Kayhan, H. (2022). A combined method for preparation of landslide susceptibility map in Izmir (Türkiye). Applied Sciences, 12(18), 9029. https://doi.org/10.3390/app12189029

19. Roy, P., Ghosal, K., & Paul, P. K. (2022). Landslide susceptibility mapping of Kalimpong in Eastern Himalayan Region using a Rprop ANN approach. Journal of Earth System Science, 131(2), 130. https://doi.org/10.1007/s12040-022-01877-2

20. Sweta, K., Goswami, A., Nath, R. R., & Bahuguna, I. M. (2022). Performance assessment for three statistical models of landslide susceptibility zonation mapping: A case study for Dharamshala Region, Himachal Pradesh, India. Journal of Earth System Science, 131(3), 143. https://doi.org/10.1007/s12040-022-01881-6

21. Khusulio, K., & Kumar, R. (2023). Feasibility assessment of multi-criteria decision making and quantitative landslide susceptibility methods: A case study of Mao-Maram Manipur. Journal of Earth System Science, 132(2), 56. https://doi.org/10.1007/s12040-023-02062-9

22. Som, S. K., Ghosh, S., Dasgupta, S., Kumar, N. T., Hindayar, J. N., Mohan, M., ... & Bhattacharya, S. (2023). Utility of common variance of equally-weighted variables for GIS-based landslide susceptibility mapping at the eastern Himalaya. Journal of Earth System Science, 132(1), 16. https://doi.org/10.1007/s12040-022-02017-6

23. Guzzetti, F., Galli, M., Reichenbach, P., Ardizzone, F., & Cardinali, M. J. N. H. (2006). Landslide hazard assessment in the Collazzone area, Umbria, Central Italy. Natural Hazards and Earth System Sciences, 6(1), 115-131. https://doi.org/10.5194/nhess-6-115-2006

24. Erener, A., Mutlu, A., & Düzgün, H. S. (2016). A comparative study for landslide susceptibility mapping using GIS-based multi-criteria decision analysis (MCDA), logistic regression (LR) and association rule mining (ARM). Engineering Geology, 203, 45-55. https://doi.org/10.1016/j.enggeo.2015.09.007

25. Loche, M., Alvioli, M., Marchesini, I., Bakka, H., & Lombardo, L. (2022). Landslide susceptibility maps of Italy: Lesson learnt from dealing with multiple landslide types and the uneven spatial distribution of the national inventory. Earth-Science Reviews, 232, 104125. https://doi.org/10.1016/j.earscirev.2022.104125

26. Liu, S., Wang, L., Zhang, W., Sun, W., Fu, J., Xiao, T., & Dai, Z. (2023). A physics-informed data-driven model for landslide susceptibility assessment in the Three Gorges Reservoir Area. Geoscience Frontiers, 14(5), 101621. https://doi.org/10.1016/j.gsf.2023.101621

27. Luo, W., & Liu, C. C. (2018). Innovative landslide susceptibility mapping supported by geomorphon and geographical detector methods. Landslides, 15, 465-474. https://doi.org/10.1007/s10346-017-0893-9

28. Akinci, H., & Yavuz Ozalp, A. (2021). Landslide susceptibility mapping and hazard assessment in Artvin (Turkey) using frequency ratio and modified information value model. Acta Geophysica, 69(3), 725-745. https://doi.org/10.1007/s11600-021-00577-7

29. Pradhan, B. (2011). Use of GIS-based fuzzy logic relations and its cross application to produce landslide susceptibility maps in three test areas in Malaysia. Environmental Earth Sciences, 63(2), 329-349. https://doi.org/10.1007/s12665-010-0705-1

30. Kumar, R., & Anbalagan, R. (2016). Landslide susceptibility mapping using analytical hierarchy process (AHP) in Tehri reservoir rim region, Uttarakhand. Journal of the Geological Society of India, 87, 271-286. https://doi.org/10.1007/s12594-016-0395-8

31. Fatemi Aghda, S. M., Bagheri, V., & Razifard, M. (2018). Landslide susceptibility mapping using fuzzy logic system and its influences on mainlines in lashgarak region, Tehran, Iran. Geotechnical and Geological Engineering, 36, 915-937. https://doi.org/10.1007/s10706-017-0365-y

32. Mandal, S., Mondal, S., Mandal, S., & Mondal, S. (2019). Frequency ratio (FR) model and modified information value (MIV) model in landslide susceptibility assessment and prediction. Statistical Approaches for Landslide Susceptibility Assessment and Prediction, 77-105. https://doi.org/10.1007/978-3-319-93897-4_3

33. Okoli, J., Nahazanan, H., Nahas, F., Kalantar, B., Shafri, H. Z. M., & Khuzaimah, Z. (2023). High-Resolution lidar-derived DEM for landslide susceptibility assessment using AHP and fuzzy logic in Serdang, Malaysia. Geosciences, 13(2), 34. https://doi.org/10.3390/geosciences13020034

34. Ünel, F. B., Kuşak, L., Yakar, M., & Doğan, H. (2023). Coğrafi bilgi sistemleri ve analitik hiyerarşi prosesi kullanarak Mersin ilinde otomatik meteoroloji

gözlem istasyonu yer seçimi. Geomatik, 8(2), 107-123. https://doi.org/10.29128/geomatik.1136951

35. Pourghasemi, H. R., Mohammady, M., & Pradhan, B. (2012). Landslide susceptibility mapping using index of entropy and conditional probability models in GIS: Safarood Basin, Iran. Catena, 97, 71-84. https://doi.org/10.1016/j.catena.2012.05.005

36. Achour, Y., Boumezbeur, A., Hadji, R., Chouabbi, A., Cavaleiro, V., & Bendaoud, E. A. (2017). Landslide susceptibility mapping using analytic hierarchy process and information value methods along a highway road section in Constantine, Algeria. Arabian Journal of Geosciences, 10, 194. https://doi.org/10.1007/s12517-017-2980-6

37. Kohno, M., & Higuchi, Y. (2023). Landslide susceptibility assessment in the Japanese archipelago based on a landslide distribution map. ISPRS International Journal of Geo-Information, 12(2), 37. https://doi.org/10.3390/ijgi12020037

38. Zhu, L., & Huang, J. F. (2006). GIS-based logistic regression method for landslide susceptibility mapping in regional scale. Journal of Zhejiang University-Science A, 7(12), 2007-2017. https://doi.org/10.1631/jzus.2006.A2007

39. Akgun, A. (2012). A comparison of landslide susceptibility maps produced by logistic regression, multi-criteria decision, and likelihood ratio methods: a case study at İzmir, Turkey. Landslides, 9(1), 93-106. https://doi.org/10.1007/s10346-011-0283-7

40. Rasyid, A. R., Bhandary, N. P., & Yatabe, R. (2016). Performance of frequency ratio and logistic regression model in creating GIS based landslides susceptibility map at Lompobattang Mountain, Indonesia. Geoenvironmental Disasters, 3, 1-16. https://doi.org/10.1186/s40677-016-0053-x

41. Polykretis, C., & Chalkias, C. (2018). Comparison and evaluation of landslide susceptibility maps obtained from weight of evidence, logistic regression, and artificial neural network models. Natural Hazards, 93, 249-274. https://doi.org/10.1007/s11069-018-3299-7

42. Wubalem, A., & Meten, M. (2020). Landslide susceptibility mapping using information value and logistic regression models in Goncha Siso Eneses area, northwestern Ethiopia. SN Applied Sciences, 2, 1-19. https://doi.org/10.1007/s42452-020-2563-0

43. Sekarlangit, N., Fathani, T. F., & Wilopo, W. (2022). Landslide susceptibility mapping of Menoreh Mountain using logistic regression. Journal of Applied Geology, 7(1), 51-63. https://doi.org/10.22146/jag.72067

44. Yadav, M., Pal, S. K., Singh, P. K., & Gupta, N. (2023). Landslide susceptibility zonation mapping using frequency ratio, information value model, and logistic regression model: a case study of Kohima district in Nagaland, India. In Landslides: Detection, Prediction and Monitoring: Technological Developments, 333-363. https://doi.org/10.1007/978-3-031-23859-8_17

45. Lee, S., & Sambath, T. (2006). Landslide susceptibility mapping in the Damrei Romel area, Cambodia using frequency ratio and logistic regression models. Environmental Geology, 50, 847-855. https://doi.org/10.1007/s00254-006-0256-7

46. Yilmaz, I. (2009). Landslide susceptibility mapping using frequency ratio, logistic regression, artificial neural networks and their comparison: a case study from Kat landslides (Tokat—Turkey). Computers & Geosciences, 35(6), 1125-1138. https://doi.org/10.1016/j.cageo.2008.08.007

47. Akinci, H., Doğan, S., Kiliçoğlu, C., & Temiz, M. S. (2011). Production of landslide susceptibility map of Samsun (Turkey) City Center by using frequency ratio method. International Journal of the Physical Sciences, 6(5), 1015-1025. https://doi.org/10.5897/IJPS11.133

48. Karaman, M. O., Çabuk, S. N., & Pekkan, E. (2022). Utilization of frequency ratio method for the production of landslide susceptibility maps: Karaburun Peninsula case, Turkey. Environmental Science and Pollution Research, 29(60), 91285-91305. https://doi.org/10.1007/s11356-022-21931-2

49. Addis, A. (2023). GIS-Based landslide susceptibility mapping using frequency ratio and Shannon Entropy Models in Dejen District, Northwestern Ethiopia. Journal of Engineering, 2023(1), 1062388. https://doi.org/10.1155/2023/1062388

50. Ba, Q., Chen, Y., Deng, S., Wu, Q., Yang, J., & Zhang, J. (2017). An improved information value model based on gray clustering for landslide susceptibility mapping. ISPRS International Journal of Geo-Information, 6(1), 18. https://doi.org/10.3390/ijgi6010018

51. Du, G. L., Zhang, Y. S., Iqbal, J., Yang, Z. H., & Yao, X. (2017). Landslide susceptibility mapping using an integrated model of information value method and logistic regression in the Bailongjiang watershed, Gansu Province, China. Journal of Mountain Science, 14, 249-268. https://doi.org/10.1007/s11629-016-4126-9

52. Mandal, B., & Mandal, S. (2017). Landslide susceptibility mapping using modified information value model in the Lish river basin of Darjiling Himalaya. Spatial Information Research, 25, 205-218. https://doi.org/10.1007/s41324-017-0096-4

53. Khan, H., Shafique, M., Khan, M. A., Bacha, M. A., Shah, S. U., & Calligaris, C. (2019). Landslide susceptibility assessment using Frequency Ratio, a case study of northern Pakistan. The Egyptian Journal of Remote Sensing and Space Science, 22(1), 11-24. https://doi.org/10.1016/j.ejrs.2018.03.004

54. Jadda, M., Shafri, H. Z., Mansor, S. B., Sharifikia, M., & Pirasteh, S. (2009). Landslide susceptibility evaluation and factor effect analysis using probabilistic-frequency ratio model. European Journal of Scientific Research, 33(4), 654-668.

55. Jaafari, A., Najafi, A., Pourghasemi, H. R., Rezaeian, J., & Sattarian, A. (2014). GIS-based frequency ratio and index of entropy models for landslide susceptibility assessment in the Caspian forest, northern Iran. International Journal of Environmental Science and Technology, 11, 909-926.

https://doi.org/10.1007/s13762-013-0464-0

56. Liu, L. L., Zhang, Y. L., Xiao, T., & Yang, C. (2022). A frequency ratio–based sampling strategy for landslide susceptibility assessment. Bulletin of Engineering Geology and the Environment, 81(9), 360. https://doi.org/10.1007/s10064-022-02836-3

57. Alam, A., Ahmed, B., Sammonds, P., & Kamal, A. M. (2023). Applying rainfall threshold estimates and frequency ratio model for landslide hazard assessment in the coastal mountain setting of South Asia. Natural Hazards Research, 3(3), 531-545. https://doi.org/10.1016/j.nhres.2023.08.002

58. Singh, P., Sur, U., Rai, P. K., & Singh, S. K. (2023). Landslide susceptibility prediction using frequency ratio model: a case study of Uttarakhand, Himalaya (India). Proceedings of the Indian National Science Academy, 89(3), 600-612. https://doi.org/10.1007/s43538-023-00171-z

59. Thambidurai, P., Veerappan, R., Beigh, I. H., & Luitel, K. K. (2023). Landslide susceptibility assessment using frequency ratio model in Turung Mamring, south district of Sikkim, India. In Landslides: Detection, Prediction and Monitoring: Technological Developments, 285-305. https://doi.org/10.1007/978-3-031-23859-8_14

60. Kadi, F. (2024). Statistical-based models for the production of landslide susceptibility maps and general risk analyses: a case study in Maçka, Turkey. Acta Geophysica, 1-26. https://doi.org/10.1007/s11600-024-01380-w

61. Tampekis, S., Sakellariou, S., Samara, F., Sfougaris, A., Jaeger, D., & Christopoulou, O. (2015). Mapping the optimal forest road network based on the multicriteria evaluation technique: the case study of Mediterranean Island of Thassos in Greece. Environmental Monitoring and Assessment, 187, 1-17. https://doi.org/10.1007/s10661-015-4876-9

62. Picchio, R., Pignatti, G., Marchi, E., Latterini, F., Benanchi, M., Foderi, C., ... & Verani, S. (2018). The application of two approaches using GIS technology implementation in forest road network planning in an Italian mountain setting. Forests, 9(5), 277. https://doi.org/10.3390/f9050277

63. Çölkuşu, T., & Buğday, E. (2022). Planning optimal forest road network using unmanned aerial vehicle (Eldivan Sample). 1st International Karatekin Science and Technology Conference, 199-204.

64. Taş, İ., Kaska, M. S., & Akay, A. E. (2023). Assessment of using UAV photogrammetry based DEM and ground-measurement based DEM in computer-assisted forest road design. European Journal of Forest Engineering, 9(1), 1-9. https://doi.org/10.33904/ejfe.1312514

65. Boston, K. (2016). The potential effects of forest roads on the environment and mitigating their impacts. Current Forestry Reports, 2, 215-222. https://doi.org/10.1007/s40725-016-0044-x

66. AFAD, (2019). Overview of Disaster Management and Natural Disaster Statistics. https://en.afad.gov.tr/kurumlar/en.afad/Afet_Istatistikleri_2020_eng_1.pdf

67. Akgün, A. (2018). Bulanık uyarlanabilir rezonans teorisi (FuzzyART) yöntemi kullanılarak heyelan duyarlılık analizi: Tonya (Trabzon) Örneği. Gümüşhane Üniversitesi Fen Bilimleri Dergisi, 8(1), 135-146. https://doi.org/10.17714/gumusfenbil.346532

68. http://www.tonya.gov.tr/ilcemizin-cografi-durumuu

69. Abeysiriwardana, H. D., & Gomes, P. I. (2022). Integrating vegetation indices and geo-environmental factors in GIS-based landslide-susceptibility mapping: using logistic regression. Journal of Mountain Science, 19(2), 477-492. https://doi.org/10.1007/s11629-021-6988-8

70. Wang, X., Huang, F., Fan, X., Shahabi, H., Shirzadi, A., Bian, H., ... & Chen, W. (2022). Landslide susceptibility modeling based on remote sensing data and data mining techniques. Environmental Earth Sciences, 81(2), 50. https://doi.org/10.1007/s12665-022-10195-1

71. Kanwal, S., Atif, S., & Shafiq, M. (2017). GIS based landslide susceptibility mapping of northern areas of Pakistan, a case study of Shigar and Shyok Basins. Geomatics, Natural Hazards and Risk, 8(2), 348-366. https://doi.org/10.1080/19475705.2016.1220023

72. Ali, S. A., Parvin, F., Vojteková, J., Costache, R., Linh, N. T. T., Pham, Q. B., ... & Ghorbani, M. A. (2021). GIS-based landslide susceptibility modeling: A comparison between fuzzy multi-criteria and machine learning algorithms. Geoscience Frontiers, 12(2), 857-876. https://doi.org/10.1016/j.gsf.2020.09.004

73. Melese, T., Belay, T., & Andemo, A. (2022). Application of analytical hierarchal process, frequency ratio, and Shannon entropy approaches for landslide susceptibility mapping using geospatial technology: The case of Dejen district, Ethiopia. Arabian Journal of Geosciences, 15(5), 424. https://doi.org/10.1007/s12517-022-09672-5

74. Rabby, Y. W., Li, Y., & Hilafu, H. (2023). An objective absence data sampling method for landslide susceptibility mapping. Scientific Reports, 13(1), 1740. https://doi.org/10.1038/s41598-023-28991-5

75. Yılmaz, O. S. (2023). Frekans oranı yöntemiyle coğrafi bilgi sistemi ortamında heyelan duyarlılık haritasının üretilmesi: Manisa, Demirci, Tekeler Köyü örneği. Geomatik, 8(1), 42-54. https://doi.org/10.29128/geomatik.1108735

76. Yalcin, A., & Bulut, F. (2007). Landslide susceptibility mapping using GIS and digital photogrammetric techniques: a case study from Ardesen (NE-Turkey). Natural Hazards, 41(1), 201-226. https://doi.org/10.1007/s11069-006-9030-0

77. Yilmaz, O. S. (2022). Flood hazard susceptibility areas mapping using Analytical Hierarchical Process (AHP), Frequency Ratio (FR) and AHP-FR ensemble based on Geographic Information Systems (GIS): A case study for Kastamonu, Türkiye. Acta Geophysica, 70(6), 2747-2769. https://doi.org/10.1007/s11600-022-00882-9

78. Moore, I. D., Grayson, R. B., & Ladson, A. R. (1991). Digital terrain modelling: a review of hydrological, geomorphological, and biological applications. Hydrological Processes, 5(1), 3-30. https://doi.org/10.1002/hyp.3360050103

79. Wang, L. J., Guo, M., Sawada, K., Lin, J., & Zhang, J. (2016). A comparative study of landslide susceptibility maps using logistic regression, frequency ratio, decision tree, weights of evidence and artificial neural network. Geosciences Journal, 20, 117-136. https://doi.org/10.1007/s12303-015-0026-1

80. Sun, X., Chen, J., Han, X., Bao, Y., Zhou, X., & Peng, W. (2020). Landslide susceptibility mapping along the upper Jinsha River, south-western China: a comparison of hydrological and curvature watershed methods for slope unit classification. Bulletin of Engineering Geology and the Environment, 79, 4657-4670. https://doi.org/10.1007/s10064-020-01849-0

81. Yılmaz, Ç. Ş. (2022). Improving the land cover mapping accuracy of the Sentinel-2 imagery on Google Earth Engine. Türk Uzaktan Algılama ve CBS Dergisi, 3(2), 150-159. https://doi.org/10.48123/rsgis.1119572

82. Althuwaynee, O. F., Pradhan, B., Park, H. J., & Lee, J. H. (2014). A novel ensemble bivariate statistical evidential belief function with knowledge-based analytical hierarchy process and multivariate statistical logistic regression for landslide susceptibility mapping. Catena, 114, 21-36. https://doi.org/10.1016/j.catena.2013.10.011

83. Gudiyangada Nachappa, T., Kienberger, S., Meena, S. R., Hölbling, D., & Blaschke, T. (2020). Comparison and validation of per-pixel and object-based approaches for landslide susceptibility mapping. Geomatics, Natural Hazards and Risk, 11(1), 572-600. https://doi.org/10.1080/19475705.2020.1736190

84. Hussain, S., Mubeen, M., Akram, W., Ahmad, A., Habib-ur-Rahman, M., Ghaffar, A., ... & Nasim, W. (2020). Study of land cover/land use changes using RS and GIS: a case study of Multan district, Pakistan. Environmental Monitoring and Assessment, 192, 1-15. https://doi.org/10.1007/s10661-019-7959-1

85. Chen, X., & Chen, W. (2021). GIS-based landslide susceptibility assessment using optimized hybrid machine learning methods. Catena, 196, 104833. https://doi.org/10.1016/j.catena.2020.104833

86. Hakim, W. L., Rezaie, F., Nur, A. S., Panahi, M., Khosravi, K., Lee, C. W., & Lee, S. (2022). Convolutional neural network (CNN) with metaheuristic optimization algorithms for landslide susceptibility mapping in Icheon, South Korea. Journal of Environmental Management, 305, 114367. https://doi.org/10.1016/j.jenvman.2021.114367

87. Chen, W., & Yang, Z. (2023). Landslide susceptibility modeling using bivariate statistical-based logistic regression, naïve Bayes, and alternating decision tree models. Bulletin of Engineering Geology and the Environment, 82(5), 190. https://doi.org/10.1007/s10064-023-03216-1

88. Yu, C., Lee, J. A. Y., & Munro-Stasiuk, M. J. (2003). Extensions to least-cost path algorithms for roadway planning. International Journal of Geographical Information Science, 17(4), 361-376. https://doi.org/10.1080/1365881031000072645

89. Effat, H. A., & Hassan, O. A. (2013). Designing and evaluation of three alternatives highway routes using the Analytical Hierarchy Process and the least-cost path analysis, application in Sinai Peninsula, Egypt. The Egyptian Journal of Remote Sensing and Space Science, 16(2), 141-151. https://doi.org/10.1016/j.ejrs.2013.08.001

90. McDonald, M. D., & Kessler, F. C. (2022). Least-Cost path and accessibility analysis of a high speed railway corridor: Victorville, CA to Las Vegas, NV. Journal of Geographic Information System, 14(1), 40-60. https://doi.org/10.4236/jgis.2022.141003

91. Sawant, S., & Sawant, S. (2023). Finding optimal path for gas pipeline using GIS and RS. Proceedings of the International Conference on Cognitive and Intelligent Computing: ICCIC 2021, 2, 321-333. https://doi.org/10.1007/978-981-19-2358-6_31